



Photoluminescence of gallium ion irradiated hexagonal and cubic GaN quantum dots



Charlotte Rothfuchs^{a,*}, Nadezhda Kukharchyk^a, Tristan Koppe^b, Fabrice Semond^c, Sarah Blumenthal^d, Hans-Werner Becker^e, Donat J. As^d, Hans C. Hofsäuss^b, Andreas D. Wieck^a, Arne Ludwig^a

^a Lehrstuhl für Angewandte Festkörperphysik, Ruhr-Universität Bochum, Universitätsstraße 150, D-44780 Bochum, Germany

^b II. Physikalisches Institut, Georg-August-Universität Göttingen, Friedrich-Hund-Platz 1, D-37077 Göttingen, Germany

^c CNRS-CRHEA, Rue Bernard Grégory, F-06560 Valbonne, France

^d Department Physik, Universität Paderborn, Warburger Straße 100, D-33098 Paderborn, Germany

^e RUBION, Ruhr-Universität Bochum, Universitätsstraße 150, D-44780 Bochum, Germany

ARTICLE INFO

Article history:

Received 15 April 2016

Received in revised form 3 May 2016

Accepted 6 June 2016

Keywords:

GaN/AlN

Quantum dots

Ion beam implantation

Photoluminescence

Quantum confined Stark effect

ABSTRACT

We report on ion implantation into GaN QDs and investigate their radiation hardness. The experimental study is carried out by photoluminescence (PL) measurements on molecular beam epitaxy-grown GaN quantum dots after ion implantation. Both quantum dots grown in the hexagonal (H) and the cubic (C) crystal structure were subjected to gallium ions with an energy of 400 kV (H) and 75 kV (C) with fluences ranging from $5 \times 10^{10} \text{ cm}^{-2}$ to $1 \times 10^{14} \text{ cm}^{-2}$ (H) and to $1 \times 10^{15} \text{ cm}^{-2}$ (C), respectively. Low-temperature PL measurements reveal a PL quenching for which a quantitative model as a function of the ion fluence is developed. A high degradation resistance is concluded. A non-radiative trap with one main activation energy is found for all QD structures by temperature-dependent PL measurements. Further analysis of fluence-dependent PL energy shifts shows ion-induced intermixing and strain effects. Particular for the hexagonal quantum dots, a strong influence of the quantum confined Stark effect is present.

© 2016 Elsevier B.V. All rights reserved.

1. Introduction

The growth of GaN quantum dots (QD) started in the second half of the 1990s overcoming main difficulties with the growth quality for the first time [1]. Since then, great progress in the fabrication and investigation of GaN QDs with the prospect of electrical and optical device applications was initiated. They are promising candidates for light emitters covering a wide spectral range from the ultraviolet and blue to the orange range [2,3]. Moreover, they offer excellent quantum efficiency even at room temperature due to the large exciton binding energy and strong quantum confinement [3]. This opens new perspectives in device applications like UV-lasers and intersubband transition devices working in the near-infrared region [1,4]. Recently, also progress in GaN QDs based single-photon emission for quantum cryptography was reported. It was measured both for hexagonal and cubic GaN QDs in single etched mesa-structures [5,6]. Besides, also GaN QDs grown on quantum well structures were observed as single quantum emitters [7]. Another option for the realization of

a single-photon source could be the post-selection of single GaN QDs by a disabling of all QDs around an intentional one using local focused ion beam implantation [8]. For this, a detailed knowledge about the QDs degradation resistance and the further ion impact on these nanostructures is necessary.

A further interest of quantum communication technology in a well-understood response of the QDs to ion irradiation arises for spin-electronic QD devices [9]. These could be realized by injection of magnetic dopants into GaN QDs, for which the QDs are required to be radiation hard. Successful demonstrations of annealed manganese ion-implanted p-GaN with a subsequent ferromagnetic behaviour and a very high Curie temperature of $\sim 250 \text{ K}$ already show the great potential of GaN based spintronic devices [10].

Here, we investigate gallium (Ga) ion implantation into GaN/AlN QDs grown in the hexagonal as well as in the cubic crystal structure and carry out photoluminescence (PL) measurements on irradiated QD ensembles, as described in chapter 2. In chapter 3.1, the low-temperature PL is quantitatively described with a fluence-dependent model developed by us under the assumption of an implantation-induced creation of non-radiative traps. Corresponding thermally activated non-radiative processes are studied in chapter 3.3 by temperature-dependent PL and

* Corresponding author.

E-mail address: Charlotte.Rothfuchs@ruhr-uni-bochum.de (C. Rothfuchs).

non-radiative traps with one main activation energy are determined. Additional ion-induced changes in the PL energy are credited with atom intermixing and a strong influence of the quantum confined Stark effect in the samples with hexagonal crystal structure, as discussed in chapter 3.2. Furthermore, strain effects are taken into account for all structure types.

2. Materials and methods

2.1. Sample structures and properties

The GaN QDs were grown by molecular beam epitaxy in the Stranski–Krastanov growth mode in both the hexagonal (wurtzite) and the cubic (zinc-blende) crystal structure. In the following, we speak of hexagonal and cubic QDs. The hexagonal QDs are embedded in an AlN matrix extending to 400 nm below the quantum dots to the Si(111) substrate and to 150 nm on top to the surface. Two samples, one with a QD density of about 10^{10} cm^{-2} (sample H1) and a second one with a lower density of $5 \times 10^9 \text{ cm}^{-2}$ (sample H2), were studied, where the QDs have bottom lengths between 22 nm and 29 nm and heights of about 1.7 nm according to AFM measurements on surface QDs. The sample structure is schematically shown in Fig. 1(a). In these hexagonal heterostructures, an internal electric field leads to a huge quantum confined Stark effect (QCSE) due to spontaneous and piezoelectric polarizations. Consequently, band bending occurs with a spatial separation of electrons and holes and a reduced radiative recombination efficiency [11,12]. This is illustrated by a three-dimensional calculation of the band structure shown in Fig. 1(a), simulated with the nextnano software [13].

The cubic QDs (sample C), sketched in Fig. 1(b), were grown on Si(001) substrate, which was first covered by a $10 \mu\text{m}$ thick layer of 3C-SiC and a 30 nm thick AlN buffer. A 30 nm thick AlN capping layer was grown on top of the QDs, which have a density of about $8 \times 10^{10} \text{ cm}^{-2}$ [14]. In this cubic material system, we assume a background doping in the order of 10^{17} cm^{-3} due to residual oxygen contamination. Further, a weak piezoelectric field and band bending are expected [15].

2.2. Ion implantation and characterization

The implantation of the hexagonal QDs was performed with a 4 MV Dynamitron tandem accelerator using a 400 keV Ga ion beam. Areas of $\sim 0.8 \text{ mm}^2$ were irradiated with a current density of about $3.6 \text{ nA}\cdot\text{cm}^{-2}$ and with fluences ranging from $1 \times 10^{11} \text{ cm}^{-2}$ to $1 \times 10^{14} \text{ cm}^{-2}$ for sample H1 and from $5 \times 10^{10} \text{ cm}^{-2}$ to $5 \times 10^{13} \text{ cm}^{-2}$ for sample H2. On the cubic sample C, implantation areas of 1 mm^2 were scanned in an EIKO-100 FIB system with 75 keV Ga ions and a current density between $27.1 \text{ nA}\cdot\text{cm}^{-2}$ and $0.2 \text{ nA}\cdot\text{cm}^{-2}$ in a fluence range from $5 \times 10^{10} \text{ cm}^{-2}$ to $1 \times 10^{15} \text{ cm}^{-2}$. For both implantation experiments, the ion-induced displacements as a function of the target depth were simulated with the SRIM software [16] and are additionally plotted in Fig. 1. An average defect number of $2.3 (\text{Ion}\cdot\text{\AA})^{-1}$ (H1, H2) and $2.6 (\text{Ion}\cdot\text{\AA})^{-1}$ (C) is determined in the QD layer.

All irradiated samples were characterized by photoluminescence (PL) measurements from low temperature (18 K) up to room temperature. The PL setup was equipped with a titanium-sapphire laser pumped by a 10 W 532 nm semiconductor laser offering an output power of more than 1.3 W (800 nm) with a pulse repetition rate of 76 MHz. An additional harmonics generator enabled generation of the third-harmonic with a wavelength of $\sim 266 \text{ nm}$ and a power of about 30 mW, which was used as excitation source. The

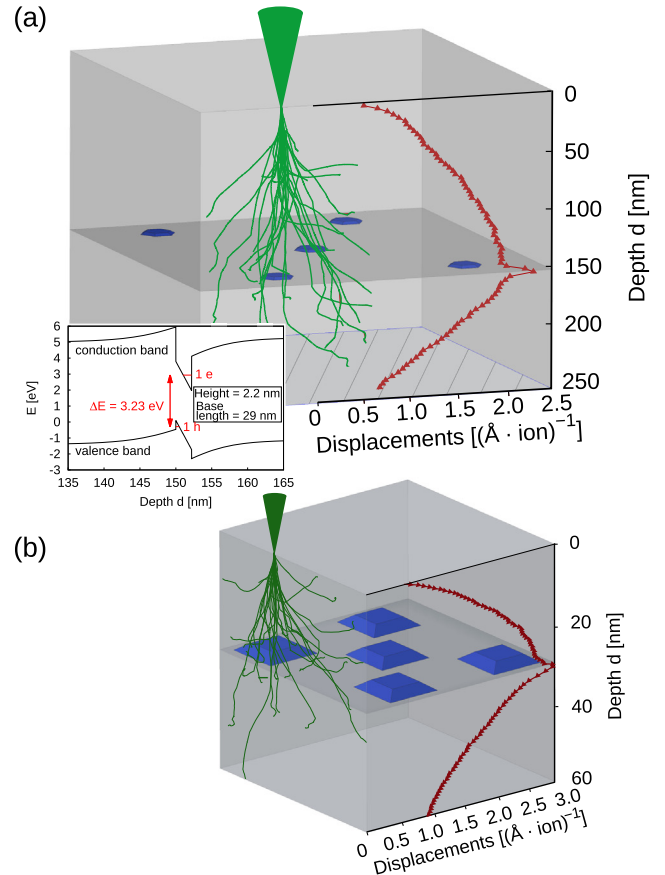


Fig. 1. Schematics of the samples with hexagonal GaN QDs (a) and cubic GaN QDs (b), both embedded in an AlN matrix. A SRIM simulation [16] of the ion-induced damage profile is depicted in red and Ga ion trajectories simulated with the Iradina software [17] are plotted in green. The additional inset in (a) shows the band energy diagram for the hexagonal QD structure calculated with the nextnano software [13]. (For interpretation of the references to colour in this figure legend, the reader is referred to the web version of this article.)

signal was recorded by a SPEX 1000 mm spectrometer coupled to a nitrogen cooled CCD system.

3. Results

3.1. Fluence-dependent PL intensity

First, PL measurements at low temperature will be discussed. In Fig. 2(a) the PL spectra measured at 18 K for ensembles with hexagonal QDs irradiated with different fluences are plotted. Corresponding results for the cubic QDs are shown in Fig. 3(a). For all kinds of samples it can be noted that the total PL intensity I decreases with increasing fluence Φ , which has been reported previously for other types of semiconductor QDs [18,19,8]. Nonetheless, the degradation curve does not coincide with the one observed for InAs/GaAs QDs, for which a model of the form [8]

$$\frac{fI}{fI_0} = \frac{1}{1 + \kappa \cdot \Phi}, \quad (1)$$

was developed, where I_0 denotes the initial PL intensity and κ is a proportionality constant. The model is based on the assumption that the quantum efficiency and the directly related PL intensity, according to $fI \propto 1/(1 + R_n/R_r)$, are mainly quenched by the defect-assisted non-radiative recombination rate R_n increasing linearly with the ion fluence. Yet, for the fluence range investigated

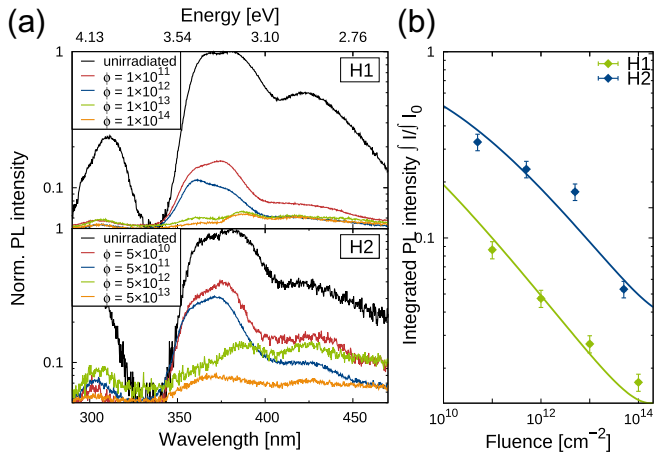


Fig. 2. (a) PL spectra measured at 18 K for hexagonal QD ensembles irradiated with different fluences. We attribute all of the peaks to QD luminescence and explicitly verified that it is not due to luminescence of defects in the AlN matrix. The fluence values are given in units of cm^{-2} . (b) Fluence-dependent integrated intensity for the PL spectra depicted in (a) with the adjusted model of Eq. (3). We note, that the QD density of sample H1 is higher than of sample H2.

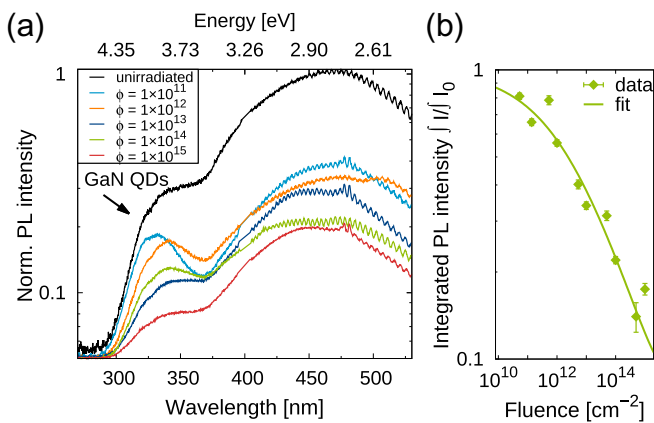


Fig. 3. (a) PL spectra measured at 18 K for cubic QD ensembles irradiated with different fluences. The unit of the fluence values is cm^{-2} . (b) Integrated PL intensity extracted from (a) as a function of the ion fluence. The model of Eq. (3) is fitted to the data. The PL peak of the cubic GaN QDs is located at around 332 nm (3.74 eV).

here, it is important to consider that the initial linear fluence-dependent increase of the defect concentration N_d at low fluences saturates in the higher fluence range. This is caused by a damage overlap and a recombination of point defects [20,21]. Then, the total non-radiative recombination rate can be modeled by a function of the form $R_n = R_{n,0} + \tilde{p}/r \cdot (1 - \exp(-r \cdot \Phi))$ [22], with the initial non-radiative recombination rate $R_{n,0}$. The constants \tilde{p} and r are measures for the cross sections of production and recombination of point defects and depend on the QD density and induced defect concentration in the QD structures.

Additionally, for a complete description of the fluence-dependent PL of the GaN QDs, it is essential to take into account a change in the radiative recombination rate R_r with respect to the quantum confined Stark effect (QCSE). An implantation-induced alteration of the internal electric field and the QCSE has been already observed. Davis et al. [23] stated a smaller QCSE after ion implantation into $\text{ZnO}/\text{Zn}_{0.7}\text{Mg}_{0.3}\text{O}$ quantum wells due to atom intermixing in the sample. In general, radiation enhanced diffusion processes are well known for implanted III-V semiconductor heterostructures [24,25]. Thus, we consider here an aluminum and gallium diffusion process between the QDs and their vicinity.

This is suggested to lead to a decreased internal electric field F being linked up to the electron and hole wave function overlap $S_{e,h}$, which is itself proportional to the radiative recombination rate R_r . Furthermore, we assume that the interdiffusion is rather a two-dimensional effect occurring through the top and bottom QD plane due to the flat disk QD shape. In our approach, the radiative recombination rate R_r becomes then a two-third order power function of the induced three-dimensional defect density N_d and the ion fluence Φ , respectively as follows:

$$\begin{aligned} R_r &\sim S_{e,h} = f(F) \\ &= R_{r,0} \cdot (1 + \tilde{a} \cdot N_d^{2/3}) \\ &= R_{r,0} \cdot (1 + a \cdot \Phi^{2/3}), \end{aligned} \quad (2)$$

where a and \tilde{a} are substrate-dependent proportionality constants accounting for piezoelectric effects. Assuming a small initial non-radiative recombination rate compared to the radiative one ($R_{n,0} \ll R_r$), the extended model for the implantation-induced alteration of the PL intensity of the GaN QDs takes the form:

$$\frac{\int I}{\int I_0} = \frac{1}{1 + \frac{p/r \cdot (1 - \exp(-r \cdot \Phi))}{1 + a \cdot \Phi^{2/3}}}. \quad (3)$$

This model is fitted to the integrated PL intensity, resulting from a Gaussian curve-fitting to the PL peaks in Figs. 2(a) and 3(a). The data are depicted in Fig. 2(b) for the hexagonal QDs and in Fig. 3(b) for the cubic QDs. For the samples H1 and H2 the model was fitted to the experimental data by varying the value a simultaneously for both samples but by allowing individual p and r values accounting for the dependence of the non-radiative center influence on the QD density [26]. It yields $a_{H1,H2} = 0.67 \text{ cm}^{4/3}$ and $p_{H1} = 1.3 \times 10^{-3} \text{ cm}^2$, $p_{H2} = 3.0 \times 10^{-4} \text{ cm}^2$, $r_{H1} = 4.3 \times 10^{-15} \text{ cm}^2$ and $r_{H2} = 1.5 \times 10^{-15} \text{ cm}^2$. For sample C the parameters are determined to be $a_c = 0.0072 \text{ cm}^{4/3}$ and $p_c = 5.1 \times 10^{-7} \text{ cm}^2$ and $r_c = 1.1 \times 10^{-16} \text{ cm}^2$. It can be remarked, that the model describes the experimental data quite well and reveals a greater change of the QCSE by the Ga implantation with a stronger influence on the radiative recombination rate in the hexagonal QDs. This result meets the previous expectations. An important further remark at this point is, that model-based predictions about the PL are only valid up to fluences in the range of the amorphous threshold. This threshold was experimentally determined to occur at around 100 displacements per atom (DPA) for hexagonal GaN [27] and to be about 40 times higher for hexagonal AlN [28] with 4000 DPA. These values are assumed to be nearly of the same order of magnitude for each of the cubic materials [29]. The corresponding amorphization fluences for the implantations here are calculated by using the SRIM software [16] to be around $\sim 5 \times 10^{16} \text{ cm}^{-2}$ for GaN and $\sim 1 \times 10^{18} \text{ cm}^{-2}$ for AlN. Taking this into account, our result underlines the strong degradation resistance or equivalently radiation hardness of GaN QDs compared to InAs/GaAs QDs [8]. Approaching the threshold of amorphization at irradiation fluences of 10^{14} cm^{-2} , the GaN QDs still show 10% of the initial PL signal. Contrary, the InAs QDs exhibit a much stronger PL quenching by Ga ion bombardment with a remaining PL intensity of 10% at a much lower fluence of $\sim 10^{10} \text{ cm}^{-2}$ [8]. This is several orders of magnitude below the amorphization threshold of 2 DPA¹ corresponding to a fluence of $\sim 10^{14} \text{ cm}^{-2}$ in this experiment for GaAs [30] and 6 DPA and $\sim 5 \times 10^{14} \text{ cm}^{-2}$ for InAs [31]. Summing up here, the result of the stronger degradation resistance of GaN QDs compared to the one of InAs QDs mirrors the same trend as observed for the amorphization threshold in the corresponding bulk materials and is even more distinct for the quantum structures.

¹ The DPA values are estimated from the amorphization fluences given in [30,31] by using SRIM [16].

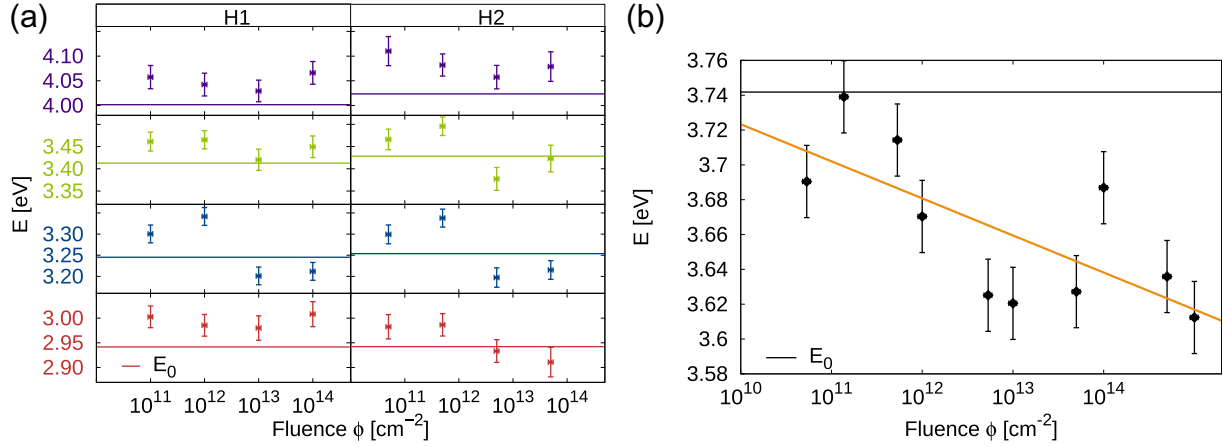


Fig. 4. Fluence-dependent PL emission energy for QDs with different sizes in the hexagonal samples H1 and H2 in (a) and for QDs with one main emission energy in the cubic sample C in (b). The solid lines represent the PL energy measured before the implantation. The orange line in (b) is plotted for guiding the eyes.

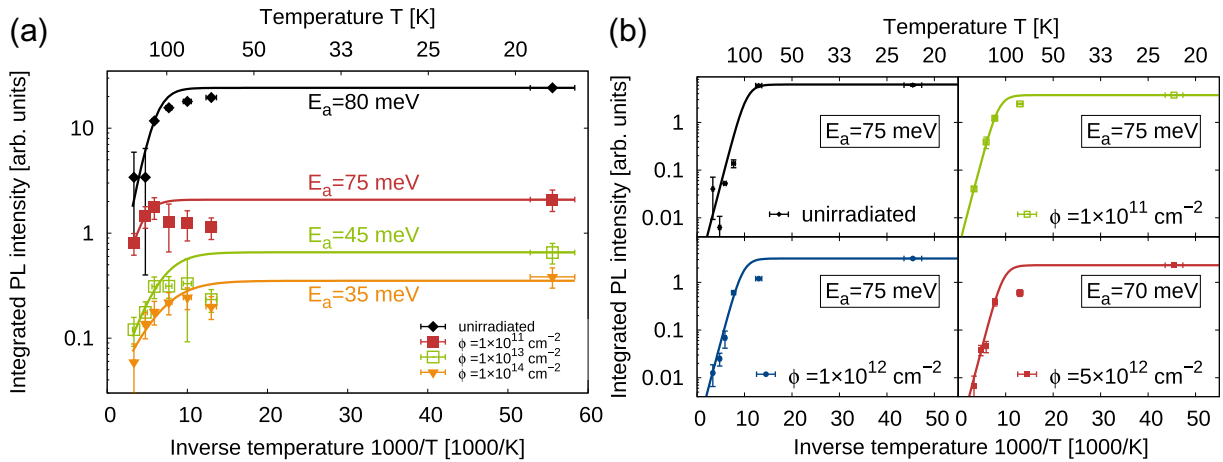


Fig. 5. Integrated PL intensity as a function of the inverse temperature for different fluence values. In (a) the results for the hexagonal QD samples and in (b) the measured data for the cubic QD samples are plotted, both along with the adjusted model of Eq. (4).

3.2. Fluence-dependent PL energy shift

Apart from the PL intensities, the shift of the PL energy, which is determined by the moved center of the fitted Gaussian curves, is analyzed. We start the discussion with the hexagonal QDs. The data are plotted in Fig. 4(a), where the individual colored lines mark the initial emission energy before the implantation and the data points show the ones measured afterwards. Prior, it has to be mentioned, that the different corresponding peaks in the PL spectra are attributed to QDs with different sizes and heights, respectively [32]. It can be noted, that for fluences below 10^{12} cm $^{-2}$, an energy blueshift occurs for all QDs in both samples. This can be understood in terms of the ion-induced intermixing and compositional change at the QD boundaries, leading to a blurred potential profile and a quenched QCSE [23]. At fluences greater than 10^{12} cm $^{-2}$, a redshift can be observed for a subset of peaks, which could be explained by additional nonlinear strain effects caused by the implanted Ga atoms in the surrounding QD matrix [33,8]. Such strain effects with a resulting relaxation in the QDs are suggested to be the main reason for the PL redshift of the cubic QDs over the whole fluence range, illustrated in Fig. 4(b). This is in accordance with the above mentioned assumption of a comparable weak influence of the QCSE in this cubic crystal structure.

3.3. Temperature-dependent PL

Additionally to the low-temperature investigations, temperature-dependent measurements are carried out in order to analyze the carrier dynamics. The temperature-dependent PL quenching attributed to the thermal activation of the non-radiative channels is fitted by the common Arrhenius equation [34]:

$$\int I(T) d\lambda = \frac{\int I(0 \text{ K}) d\lambda}{1 + a \exp(-E_a/(k_B T))}, \quad (4)$$

with the activation energy E_a and the corresponding activation rate a . The experimental data are plotted in Fig. 5(a) for the hexagonal QDs and in Fig. 5(b) for the cubic QDs along with the model of Eq. (4) with fitted parameters. The notable s-shape of the curves in Fig. 5(a) is ascribed to a carrier trapping in localized states [35,36]. Screening effects of the polarization charges, estimated to be little, are neglected here. Those might be overcome by PL measurements under low continuous excitation. Here, we generally find one main contributing non-radiative channel for the quenching at high temperatures. Its activation energy decreases from 80 meV to 35 meV with increasing ion fluence for the hexagonal structures. Contrary, we ascertain a trap activation energy of about 75 meV for the cubic grown samples, which is independent of the ion fluence. In general, these results affirm, that the PL quenching is

related to the thermal activation of defects in the QDs or in the surrounding matrix, as it is too small for an escape of a QD charge carrier to the barrier [37]. Hence, the smaller activation energies at higher ion fluences for the hexagonal samples could be ascribed to the carrier level inside the QDs being energetically closer to the non-radiative trap level. This reflects again the previously discussed reduction of the QCSE being much stronger in the hexagonal system.

4. Conclusion

To conclude, we experimentally determined a high degradation resistance of both hexagonal and cubic self-assembled GaN QDs compared to InAs QDs. The fluence-dependent PL intensity was quantitatively described. The model includes an implantation-induced increased trap-assisted non-radiative recombination as well as an increased radiative recombination due to the reduced QCSE. Altogether, ion beam implantation is presented as an effective tool to alter the PL properties of GaN QDs, especially regarding the modification of the QDs lateral surrounding preserving the PL properties due to the radiation hardness. It offers a highly promising prospect of a variety of future applications in quantum communication technologies.

Acknowledgement

We would like to thank the BMBF-Q.com-H 16KIS0109, DFH/UFA CDFA-05-06 and the Deutsche Forschungsgemeinschaft and the Russian Foundation of Basic Research in the frame of the ICRC TRR 160 for funding. Acknowledgement is also given to the RUB Research School. Furthermore, we thank Mathieu Leroux for stimulating discussions and for the insights he gave us concerning the Stark shift. Additionally, S. Blumenthal and D. J. As would like to acknowledge financial support by the DFG graduate program GRK 1464 “Micro- and Nanostructures in Optoelectronics and Photonics”.

References

- [1] Y. Arakawa, Progress in GaN-based quantum dots for optoelectronics applications, *IEEE J. Sel. Top. Quantum Electron.* 8 (4) (2002) 823–832.
- [2] S. Sergent, B. Damilano, T. Huault, J. Brault, M. Korytov, O. Tottreau, P. Vennéguès, M. Leroux, F. Semond, J. Massies, Study of the growth mechanisms of GaN/(Al, Ga)N quantum dots: correlation between structural and optical properties, *J. Appl. Phys.* 109 (2011) 053514.
- [3] B. Damilano, N. Grandjean, F. Semond, J. Massies, M. Leroux, From visible to white light emission by GaN quantum dots on Si(111) substrate, *Appl. Phys. Lett.* 75 (7) (1999) 962–964.
- [4] L.S. Dang, G. Fishman, H. Mariette, GaN quantum dots: physics and applications, *J. Korean Phys. Soc.* 42 (2003) S657–S661.
- [5] S. Kako, C. Santori, K. Hoshino, S. Götzinger, Y. Yamamoto, Y. Arakawa, A gallium nitride single-photon source operating at 200 K, *Nat. Mater.* 5 (2006) 887–892.
- [6] S. Kako, M. Holmes, S. Sergent, M. Bürger, D.J. As, Y. Arakawa, Single-photon emission from cubic GaN quantum dots, *Appl. Phys. Lett.* 104 (2014) 011101.
- [7] M.J. Holmes, K. Choi, S. Kako, M. Arita, Y. Arakawa, Room-temperature triggered single photon emission from a III-nitride site-controlled nanowire quantum dot, *Nano Lett.* 14 (2014) 982–986.
- [8] C. Rothfuchs, N. Kukharchyk, M.K. Greff, A.D. Wiek, A. Ludwig, Altering the luminescence properties of self-assembled quantum dots in GaAs by focused ion beam implantation, *Appl. Phys. B* 122 (3) (2016) 1–6, <http://dx.doi.org/10.1007/s00340-015-6305-8>.
- [9] D.P. DiVincenzo, D. Loss, Quantum computers and quantum coherence, *J. Magn. Magn. Mater.* 200 (1999) 202–218.
- [10] N. Theodoropoulou, A.F. Hebard, M.E. Overberg, C.R. Abernathy, S.J. Pearton, S. N.G. Chu, R.G. Wilson, Magnetic and structural properties of Mn-implanted GaN, *Appl. Phys. Lett.* 78 (22) (2001) 3475–3477.
- [11] M. Leroux, N. Grandjean, M. Lüigt, J. Massies, B. Gil, P. Lefebvre, P. Bigenwald, Quantum confined Stark effect due to built-in internal polarization fields in (Al, Ga)N/GaN quantum wells, *Phys. Rev. B* 58 (1998) R13371–R13374, <http://dx.doi.org/10.1103/PhysRevB.58.R13371>.
- [12] F. Widmann, J. Simon, B. Daudin, G. Feuillet, J.L. Rouvière, N.T. Pelekanos, G. Fishman, Blue-light emission from GaN self-assembled quantum dots due to giant piezoelectric effect, *Phys. Rev. B* 58 (1998) R15989–R15992, <http://dx.doi.org/10.1103/PhysRevB.58.R15989>.
- [13] S. Birner, T. Zibold, T. Andlauer, T. Kubis, M. Sabathil, A. Trellakis, P. Vogl, Nextnano: general purpose 3-D simulations, *IEEE Trans. Electron Devices* 54 (9) (2007) 2137–2142.
- [14] T. Schupp, T. Meisch, B. Neuschl, M. Feneberg, K. Thonke, K. Lischka, D.J. As, Molecular beam epitaxy based growth of cubic GaN quantum dots, *Phys. Status Solidi (c)* 8 (5) (2011) 1495–1498, <http://dx.doi.org/10.1002/pssc.201000904>.
- [15] V.A. Fonoberov, A.A. Balandin, Excitonic properties of strained wurtzite and zinc-blende GaN/Al_xGa_{1-x}N quantum dots, *J. Appl. Phys.* 94 (11) (2003) 7178–7186, <http://dx.doi.org/10.1063/1.1623330>.
- [16] J. Ziegler, M. Ziegler, J. Biersack, SRIM – the stopping and range of ions in matter, *Nucl. Instr. Meth. Phys. Res. Sect. B* 268 (2010) 1818–1823.
- [17] C. Borschel, C. Ronning, Ion beam irradiation of nanostructures – a 3D Monte Carlo simulation code, *Nucl. Instr. Meth. Phys. Res. Sect. B* 269 (19) (2011) 2133–2138, <http://dx.doi.org/10.1016/j.nimb.2011.07.004>.
- [18] N. Sobolev, A. Cavaco, M. Carmo, M. Grundmann, F. Heinrichsdorff, D. Bimberg, Enhanced radiation hardness of InAs/GaAs quantum dot structures, *Phys. Status Solidi (b)* 224 (1) (2001) 93–96, [http://dx.doi.org/10.1002/1521-3951\(200103\)224:1<93::AID-PSSB93>3.0.CO;2-6](http://dx.doi.org/10.1002/1521-3951(200103)224:1<93::AID-PSSB93>3.0.CO;2-6).
- [19] R. Sreekumar, A. Mandal, S. Chakrabarti, S.K. Gupta, Effect of heavy ion implantation on self-assembled single layer InAs/GaAs quantum dots, *J. Phys. D: Appl. Phys.* 43 (50) (2010) 505302.
- [20] E. Wendler, W. Wesch, A. Azarov, N. Catarino, A. Redondo-Cubero, E. Alves, K. Lorenz, Comparison of low- and room-temperature damage formation in Ar ion implanted GaN and ZnO, *Nucl. Instr. Meth. Phys. Res. Sect. B* 307 (2013) 394–398, the 18th International Conference on Ion Beam Modifications of Materials (IBMM2012), <http://dx.doi.org/10.1016/j.nimb.2013.01.020>.
- [21] K. Lorenz, M. Peres, N. Franco, J.G. Marques, S.M.C. Miranda, S. Magalhães, T. Monteiro, W. Wesch, E. Alves, E. Wendler, Radiation damage formation and annealing in GaN and ZnO, *SPIE Proc.* 7940 (2011), <http://dx.doi.org/10.1117/12.879402>. 794000–794000-14.
- [22] H.G. Cooper, J.S. Koehler, J.W. Marx, Irradiation effects in Cu, Ag, and Au near 10⁴ K, *Phys. Rev.* 97 (1955) 599–607, <http://dx.doi.org/10.1103/PhysRev.97.599>.
- [23] J.A. Davis, L.V. Dao, X. Wen, C. Ticknor, P. Hannaford, V.A. Coleman, H.H. Tan, C. Jagadish, K. Koike, S. Sasa, M. Inoue, M. Yano, Suppression of the internal electric field effects in ZnO/Zn_{0.7}Mg_{0.3}O quantum wells by ion-implantation induced intermixing, *Nanotechnology* 19 (5) (2008) 055205.
- [24] I.V. Bradley, W.P. Gillin, K.P. Homewood, R.P. Webb, The effects of ion implantation on the interdiffusion coefficients in In_xGa_{1-x}As/GaAs quantum well structures, *J. Appl. Phys.* 73 (4) (1993) 1686–1692, <http://dx.doi.org/10.1063/1.353204>.
- [25] P.J. Wellmann, W.V. Schoenfeld, J.M. Garcia, P.M. Petroff, Tuning of electronic states in self-assembled InAs quantum dots using an ion implantation technique, *J. Electron. Mater.* 27 (9) (1998) 1030–1033, <http://dx.doi.org/10.1007/s11664-998-0158-4>.
- [26] D. Kim, S. Okahara, M. Nakayama, Y. Shim, Experimental verification of Förster energy transfer between semiconductor quantum dots, *Phys. Rev. B* 78 (2008) 153301, <http://dx.doi.org/10.1103/PhysRevB.78.153301>.
- [27] C. Ronning, E. Carlson, R. Davis, Ion implantation into gallium nitride, *Phys. Rep.* 351 (5) (2001) 349–385, [http://dx.doi.org/10.1016/S0370-1573\(00\)00142-3](http://dx.doi.org/10.1016/S0370-1573(00)00142-3).
- [28] P. Ruterana, M.-P. Chauvat, K. Lorenz, Mechanisms of damage formation during rare earth ion implantation in nitride semiconductors, *Jpn. J. Appl. Phys.* 52 (11S) (2013) 11NH02.
- [29] A. Ionascu-Nedelcescu, C. Carlone, A. Houdayer, H.J. von Bardeleben, J.-L. Cantin, S. Raymond, Radiation hardness of gallium nitride, *IEEE Trans. Nucl. Sci.* 49 (6) (2002) 2733–2738.
- [30] I. Jenčić, M.W. Bench, I.M. Robertson, M.A. Kirk, A comparison of the amorphization induced in Al_xGa_{1-x}As and GaAs by heavy-ion irradiation, *J. Appl. Phys.* 69 (3) (1991) 1287–1293, <http://dx.doi.org/10.1063/1.347262>.
- [31] S.J. Pearton, A.R. Von Neida, J.M. Brown, K.T. Short, L.J. Oster, U.K. Chakrabarti, Ion implantation damage and annealing in InAs, and GaP, *J. Appl. Phys.* 64 (2) (1988) 629–636, <http://dx.doi.org/10.1063/1.341952>.
- [32] D. Simeonov, A. Dussaigne, R. Butté, N. Grandjean, Complex behavior of biexcitons in GaN quantum dots due to a giant built-in polarization field, *Phys. Rev. B* 77 (2008) 075306, <http://dx.doi.org/10.1103/PhysRevB.77.075306>.
- [33] B.L. Liang, Z.M. Wang, K.A. Sablon, Y.I. Mazur, G.J. Salamo, Influence of GaAs substrate orientation on InAs quantum dots: surface morphology, critical thickness, and optical properties, *Nanoscale Res. Lett.* 2 (2007) 609–613, <http://dx.doi.org/10.1007/s11671-007-9103-3>.
- [34] M. Leroux, N. Grandjean, B. Beaumont, G. Nataf, F. Semond, J. Massies, P. Gibart, Temperature quenching of photoluminescence intensities in undoped and doped GaN, *J. Appl. Phys.* 86 (1999) 3721–3728, <http://dx.doi.org/10.1063/1.371242>.
- [35] G.-E. Wang, W.-R. Zhao, S.-Q. Chen, H. Akiyama, Z.-C. Li, J.-P. Liu, B.-P. Zhang, Strong localization effect and carrier relaxation dynamics in self-assembled InGa quantum dots emitting in the green, *Nanoscale Res. Lett.* 10 (1) (2015) 1–7, <http://dx.doi.org/10.1186/s11671-015-0772-z>.
- [36] V.K. Dixit, S. Porwal, S.D. Singh, T.K. Sharma, S. Ghosh, S.M. Oak, A versatile phenomenological model for the S-shaped temperature dependence of photoluminescence energy for an accurate determination of the exciton localization energy in bulk and quantum well structures, *J. Phys. D* 47 (6) (2014) 065103.
- [37] I.A. Aleksandrov, K.S. Zhuravlev, V.G. Mansurov, Nonradiative recombination in GaN quantum dots formed in the AlN Matrix, *Semiconductors* 43 (6) (2009) 768–774.